Physics-Based Acoustic Source Identification

Luke Calkins, Reza Khodayi-mehr, Wilkins Aquino, and Michael M. Zavlanos

***Abstract*—In this paper we propose an acoustic source identification algorithm to localize multiple sources in non-trivial domains. We capture the physics of the acoustic wave propagation via the Helmholtz partial differential equation. Given a set of noisy complex pressure measurements of an acoustic field, we formulate an optimization problem to solve for the locations, shapes, and intensities of the sources that minimize the discrepancy between the observed pressure measurements and those predicted by the model. We parametrize each source with a nonlinear function that depends on a small set of parameters, greatly reducing the dimension of the problem. We present an initialization method for the resulting nonlinear optimization problem. We present experimental results showing the ability of our method to correctly identify multiple acoustic sources in a free field domain as well as a domain with obstacles and reflecting boundaries. Moreover, we show that our method can identify more interesting properties of the source field, such as relative phase difference between sources.**

I. Introduction

Source identification refers to the estimation of the location, shape, and intensity of possibly multiple sources given a set of measurements of the quantity generated by the action of these sources [1]–[3]. In this work, we focus on acoustic source identification. In the robotics literature, this often coincides with detecting the direction of an acoustic source relative to a robot. Many methods have been proposed for this purpose. Binaural methods try to mimic the human auditory system with two microphones acting as a left and right ear. A robotic system built on this concept is presented in [4] that utilizes cross correlation to calculate time delays between a pair of microphones and orient a robot toward a perceived source. Since the information obtained with only two microphones is limited, arrays utilizing many microphones have been pursued more heavily. Time difference of arrival is a popular array processing technique in which the time delay of the received signal is calculated between pairs of microphones to determine the oncoming angle using the array geometry. In [5], an array of 8 microphones on a robot is used to point a camera at a sound source in a reverberant room. The work presented in [6] guides a robot to localize a sound source in a reverberant environment based on echo-free onset detection along with time difference of arrival. These methods perform poorly in the presence of high reverberation and are limited to Line-Of-Sight (LOS) measurements. Furthermore, they cannot identify multiple sources.

This material is based upon work supported by the National Science Foundation Graduate Research Fellowship Program under Grant No. 1644868.

Luke Calkins, Reza Khodayi-mehr, Wilkins Aquino and Michael M. Zavlanos are with the Department of Mechanical Engineering and Materials Science, Duke University, Durham, NC 27708, USA, {william.calkins, reza.khodayi.mehr, wilkins.aquino, michael.zavlanos}@duke.edu.

More sophisticated array processing techniques have also been presented in the robotics literature. The well known Multiple Emitter Signal Classification (MUSIC) method [7] estimates the direction of multiple sources through a singular value decomposition of the covariance matrix of an array of microphones. Many extensions of this algorithm have been proposed. For example, in [8], the authors address the challenge of high-power noise by using a Generalized Singular Value Decomposition (GSVD-MUSIC). This assumes that the response matrix of the array is available for different source locations which is hard to obtain in complex domains where multi-path propagation is present and when the array is not assumed to be fixed in space. A survey of acoustic source localization techniques in robotics applications is presented in [9] with an in depth discussion of these different methods.

In this paper, we propose an algorithm to solve the acoustic source identification problem in more complex domains where multi-path propagation is present and the source(s) may not be in direct LOS. Most relevant to the approach presented here are methods that incorporate the physics of the acoustic wave propagation. A popular physics-based method is time reversal. Due to the invariance of the wave equation under a time reversal operation, a set of sensors can record a source signature, reverse the signals in time and transmit them such that they synchronously converge on the original source location [10]. In [11], the authors investigate time reversal in an urban environment by simulating received signals backward in time with a Finite Difference Time Domain (FDTD) method. In [12], the authors show time reversal refocusing inside a room, and through a wall. Time reversal breaks down in the presence of multiple sources.

Optimization based approaches that incorporate the underlying wave propagation physics have been investigated in simulation. The cosparse regularization approach is discussed in [13] and specifically formulated for source localization in [14]. Many optimization based approaches discretize the wave Partial Differential Equation (PDE) with the FDTD method and solve an optimization problem for the discretized source and/or pressure field that satisfy the model while minimizing the error between measurements and model prediction. The authors in [15] show that non-LOS signals can be used to locate multiple sources behind a wall. In [16], the authors simulate source reconstruction in a 2D square domain with impedance boundary conditions. In [17], the authors consider a time harmonic field and discretize the Helmholtz PDE with the Finite Element Method (FEM). However, this work assumes an explicit mapping from source to pressure is available, which for realistic large scale problems, is not the case.

In this work, we pose the source identification problem as an inverse problem in the frequency domain that estimates the

location and intensity of possibly multiple sources in a known domain given a set of noisy pressure measurements. We formulate an optimization problem that measures the discrepancy between our observed measurements and those predicted by the Helmholtz PDE. This requires the domain geometry and boundary conditions, but does not require the computation of the response for every candidate source location as in array processing techniques (MUSIC), making it general and applicable to many different environments. We parametrize the sources with a very small set of parameters as opposed to the full discretized field [13]–[17], greatly reducing the dimension of the problem. We present real experimental results showing the ability of our approach to localize multiple acoustic sources in a non-trivial domain. To the best of our knowledge, this work presents the first optimization-based acoustic source identification algorithm investigated in practice. An additional contribution lies in the ability of our method to identify more interesting properties of the source field such as shape, intensity, and phase of each source. The existing optimization-based approaches cannot discern such details, and their use has only been investigated in simulation on simple problems.

The rest of this paper is organized as follows. In Section II, we define the acoustic source identification problem and formulate it as a nonlinear optimization problem. In Section III, we present our solution method including a computationally efficient way to calculate the gradient and a method for initialization of the nonlinear optimization problem. In Section IV we present our experimental setup and results for localization of multiple sources in a complex domain before concluding in Section V.

II. Problem Definition

A. Helmholtz Partial Differential Equation

Let $\Omega \subset \mathbb{R}^3$ denote the domain of interest. The acoustic pressure $\hat{p}(\mathbf{x}, t)$ (fluctuations around ambient pressure) as a function of space, $\mathbf{x} \in \Omega$ and time, $t \in \mathbb{R}_+$, can be captured by the 3-dimensional linear wave equation

$$\nabla^2 \hat{p} - \frac{1}{c^2}\frac{\partial^2 \hat{p}}{\partial t^2} = \hat{s} \tag{1}$$

where c is the speed of sound in the medium and $\hat{s}(\mathbf{x}, t)$ is the driving source. Applying the Fourier transform to the above equation results in the Helmholtz Equation

$$\nabla^2 p + k^2 p = s \tag{2}$$

where $k = \omega/c$ is the wave number corresponding to angular frequency ω, with p and s being the Fourier transform of the pressure and source, respectively.

After discretization of the Helmholtz PDE with the Finite Element (FE) method using a mesh with n grid points, we arrive at a linear system of equations

$$\mathbf{A}\mathbf{p} = \mathbf{R}\mathbf{s} \tag{3}$$

where $\mathbf{A} = \mathbf{K} + i\omega\mathbf{C} - \omega^2\mathbf{M}$, and $\mathbf{K}$, $\mathbf{C}$, $\mathbf{M}$ and $\mathbf{R} \in \mathbb{R}^{n\times n}$ are sparse matrices that depend on the boundary conditions and type of elements used. See [18] for details. The vectors $\mathbf{p}$, $\mathbf{s} \in \mathbb{C}^n$ are the complex valued pressure and source functions, respectively, evaluated at the nodes of the FE mesh.

In order for the PDE (2) to have a unique solution, conditions must be specified on the boundary of the domain $\partial\Omega$. For the discretized PDE (3), uniqueness means $\mathbf{A}$ is non-singular. In this paper, we work with two kinds of boundary conditions. First, the sound-hard wall corresponding to a homogeneous Neumann boundary condition, $\nabla p(\mathbf{x}) \cdot \boldsymbol{n}(\mathbf{x}) = 0,\ \mathbf{x} \in \partial\Omega_N$, where $\boldsymbol{n}(\mathbf{x})$ is the outward unit normal to the boundary and $\partial\Omega_N \subset \partial\Omega$ refers to the portion of the boundary where a Neumann condition is specified. A zero-valued Neumann condition means that acoustic waves hitting $\partial\Omega_N$ are perfectly reflected back into the domain. The second type of boundary condition encountered in this paper is the Sommerfeld radiation condition given as, $\lim_{|\mathbf{x}|\to\infty} |\mathbf{x}| \left(\frac{\partial}{\partial|\mathbf{x}|} - ik\right) p(\mathbf{x}) = 0$. This condition imposes that waves normal to the boundary travel off to infinity and are not reflected back into the domain. This boundary condition is imposed on sound absorbing boundaries or when trying to simulate a free field environment.

B. Optimization Problem

Consider m stationary microphones deployed in the domain Ω that take measurements of the pressure field $\hat{p}(\mathbf{x}, t)$. After taking the Fourier transform of the recorded signals, the vector of complex pressure measurements $\mathbf{y} \in \mathbb{C}^m$ can be extracted at the desired frequency ω. The acoustic source identification problem can now be defined as follows.

Problem 2.1 (Acoustic Source Identification): Given a set of m noisy complex pressure measurements $\mathbf{y}$, estimate the source vector $\mathbf{s}$ such that those measurements $\mathbf{y}$ are as close as possible in a least squares sense to the pressure vector predicted by the discretized Helmholtz equation (3).

Problem 2.1 can be formulated as a constrained optimization problem in the following way. Let $\mathbf{Q} \in \mathbb{R}^{m\times n}$ be a boolean matrix such that multiplication with the pressure vector $\mathbf{p}$ returns the pressure at the nodes corresponding to locations where measurements were taken. Define the cost function $\mathcal{J}(\mathbf{p}, \mathbf{s}) = \frac{1}{2}\|\mathbf{Q}\mathbf{p} - \mathbf{y}\|^2$, where the norm is taken in the complex sense, i.e., $\|\mathbf{z}\|^2 = \mathbf{z}^H\mathbf{z}$, where the superscript H denotes the complex conjugate transpose. Then we can define the following optimization problem

$$\begin{aligned} \min_{\mathbf{p},\mathbf{s}} \quad & \mathcal{J}(\mathbf{p}, \mathbf{s}) \\ \text{s.t.} \quad & \mathbf{A}\mathbf{p} = \mathbf{R}\mathbf{s}. \end{aligned} \tag{4}$$

The goal is to obtain the set of pressure and source vectors that obey the physical model while matching the observed measurements as close as possible in a least squares sense.

III. Acoustic Source Identification

A. Source Parametrization

Rather than solve problem (4) in the full space of pressure and source vectors, we can solve the problem in the reduced space of source vectors, $\mathbf{s}$, while enforcing the model. Specifically, we can use the model to represent the pressure $\mathbf{p}$ as a function of the source $\mathbf{s}$, i.e., $\mathbf{p} = \mathcal{F}(\mathbf{s}) = \mathbf{A}^{-1}\mathbf{R}\mathbf{s}$ and then move along the gradient of the cost function $\hat{\mathcal{J}}(\mathbf{s}) = \mathcal{J}(\mathcal{F}(\mathbf{s}), \mathbf{s})$ to find the source $\mathbf{s}$ that minimizes this cost

function. Based on the fact that $\mathbf{A}$ is invertible, as discussed in II-A, this mapping $\mathcal{F}$ exists and is unique.

Let $\hat{\mathbf{M}} = \mathbf{Q}\mathbf{A}^{-1}\mathbf{R}$ such that $\hat{\mathbf{M}}\mathbf{s} \in \mathbb{C}^m$ corresponds to the vector of complex pressure values at the locations where measurements were taken. Due to the size of the matrix $\mathbf{A}$ for large FE meshes, its inverse can not be formed. Instead, we will obtain the gradient of $\hat{\mathcal{J}}$ exactly with two linear system solves of size n, where n is the size of the FE mesh.[1] Assume the source $\mathbf{s}$ can be parametrized by a small set of parameters rather than the full n dimensional vector. Specifically, we assume that each individual source in the domain Ω can be represented by a simple nonlinear basis function $g(\mathbf{x};\boldsymbol{\theta})$ that depends on a low-dimensional parameter vector $\boldsymbol{\theta} \in \mathbb{R}^p$ with $p \ll n$. The specific form of g used will be discussed in the next section. Therefore, for a domain with k sources, the source function s can be formed as

$$s(\mathbf{x}) = \sum_{i=1}^{k} \beta_i g(\mathbf{x};\boldsymbol{\theta}_i) \tag{5}$$

with $\beta_i \in \mathbb{C}, 1 \leq i \leq k$ being the maximum intensity (magnitude and phase at a specific frequency) of source i and g is real-valued. The vector $\mathbf{s}$ in (3) can be formed by evaluating each $g(\mathbf{x};\boldsymbol{\theta}_i)$ at the nodes of the FE mesh and then summing them up according to (5). Let $\mathbf{g}$ denote the n dimensional vector of the function g evaluated at the FE mesh nodes. Then, the function $\hat{\mathcal{J}}$ can be written as

$$\hat{\mathcal{J}}([\boldsymbol{\theta}_1, \beta_1, \ldots, \boldsymbol{\theta}_k, \beta_k]) = \frac{1}{2}\|\hat{\mathbf{M}}\mathbf{s} - \mathbf{y}\|^2. \tag{6}$$

where $\mathbf{s}$ is formed with $[\boldsymbol{\theta}_1, \beta_1, \ldots, \boldsymbol{\theta}_k, \beta_k]$ and (5). We can now define the optimization problem to solve the acoustic source identification problem for the set of source parameters and intensities $\boldsymbol{\theta}_i$, β_i for $1 \leq i \leq k$ as

$$\begin{aligned} \min_{[\boldsymbol{\theta}_1,\beta_1,\ldots,\boldsymbol{\theta}_k,\beta_k]} \quad & \hat{\mathcal{J}}(\mathbf{s}) \\ \text{s.t.} \quad & \boldsymbol{\theta}_i \in \boldsymbol{\Theta} \\ & \beta_i \in \mathcal{B} \end{aligned} \tag{7}$$

where $\boldsymbol{\Theta}$ and $\mathcal{B}$ are feasible parameter sets for each $\boldsymbol{\theta}_i$ and β_i, respectively.

B. Gradient Derivations

By treating each source intensity $\beta_i \in \mathbb{C}$ as a two-dimensional real vector $\boldsymbol{\beta}_i = [\Re(\beta_i), \Im(\beta_i)]^T \in \mathbb{R}^2$, where $\Re(\cdot)$ and $\Im(\cdot)$ refer to the real and imaginary components of the argument respectively, we can evaluate the gradient with respect to each $\boldsymbol{\theta}_i$ and $\boldsymbol{\beta}_i$ as real partial derivatives. The partial derivatives of the cost function $\hat{\mathcal{J}}$ that need to be calculated are $\nabla_{\boldsymbol{\theta}_i}\hat{\mathcal{J}}$, $\nabla_{\Re(\beta_i)}\hat{\mathcal{J}}$, and $\nabla_{\Im(\beta_i)}\hat{\mathcal{J}}$. Expanding the norm in (6) results in $\hat{\mathcal{J}}(\mathbf{s}) = \frac{1}{2}\left(\mathbf{s}^H\hat{\mathbf{M}}^H\hat{\mathbf{M}}\mathbf{s} - \mathbf{s}^H\hat{\mathbf{M}}^H\mathbf{y} - \mathbf{y}^H\hat{\mathbf{M}}\mathbf{s} + \mathbf{y}^H\mathbf{y}\right)$. Then, since each term is a complex-valued scalar, we can rewrite $\mathbf{y}^H\hat{\mathbf{M}}\mathbf{s}$ as $\overline{(\mathbf{y}^H\hat{\mathbf{M}}\mathbf{s})^H} = \overline{\mathbf{s}^H\hat{\mathbf{M}}^H\mathbf{y}}$, where $\overline{(\cdot)}$ refers to the complex conjugate of the argument. Then since $z + \overline{z} = 2\Re(z)$ for any complex number z, we arrive at $\hat{\mathcal{J}}(\mathbf{s}) = \frac{1}{2}\left(\mathbf{s}^H\hat{\mathbf{M}}^H\mathbf{M}\mathbf{s} - 2\Re(\mathbf{s}^H\hat{\mathbf{M}}^H\mathbf{y}) + \mathbf{y}^H\mathbf{y}\right)$. Now, we can take the partial derivatives with respect to the source parameters where the vector $\mathbf{s}$ is the only term that depends on $\boldsymbol{\theta}_i$ and β_i by (5). Specifically, we have that

$$\nabla_{\theta_i}\hat{\mathcal{J}} = (\partial\mathbf{g}/\partial\boldsymbol{\theta}_i)^T\Re\left(\overline{\beta_i}\hat{\mathbf{M}}^H(\hat{\mathbf{M}}\mathbf{s} - \mathbf{y})\right) \tag{8}$$

$$\nabla_{\Re(\beta_i)}\hat{\mathcal{J}} = \mathbf{g}(\boldsymbol{\theta}_i)^T\Re(\hat{\mathbf{M}}^H(\hat{\mathbf{M}}\mathbf{s} - \mathbf{y})) \tag{9}$$

$$\nabla_{\Im(\beta_i)}\hat{\mathcal{J}} = \mathbf{g}(\boldsymbol{\theta}_i)^T\Im(\hat{\mathbf{M}}^H(\hat{\mathbf{M}}\mathbf{s} - \mathbf{y})). \tag{10}$$

As expected the gradients are real-valued. The factoring of the terms in the gradients above is important computationally. Since the inverse of the FE system matrix $\mathbf{A}$ is never explicitly formed, the product $\hat{\mathbf{M}}\mathbf{s}$ represents one $n \times n$ linear system solve (3). After the subtraction of the vector $\mathbf{y}$, $\hat{\mathbf{M}}^H(\hat{\mathbf{M}}\mathbf{s} - \mathbf{y})$ represents another linear system solve of size n. Therefore, as the optimization problem (7) is solved iteratively, the gradient can be obtained exactly with two linear system solves of size n. The rest of the gradient calculation requires just matrix-vector multiplication.

C. Initialization

The introduction of the nonlinear basis functions g cause the optimization problem (7) to be nonlinear. Due to this fact, good initialization of the problem is needed to obtain a reasonable solution and avoid getting trapped in undesirable local minima. Since we expect the area covered with sources to be small in comparison to the domain size, we expect $\|\mathbf{R}\mathbf{s}\|_2$ in (3) to be small which means $\|\mathbf{A}\mathbf{p}\|_2$ should also be small. We can define an unconstrained optimization problem

$$\min_{\mathbf{p}} \quad \|\mathbf{Q}\mathbf{p} - \mathbf{y}\|_2 + \tau\|\mathbf{A}\mathbf{p}\|_2 \tag{11}$$

where $\tau > 0$ is a regularization parameter. This problem optimizes over the pressure vector as opposed to the source vector and minimizes the discrepancy between measurements while also enforcing $\|\mathbf{R}\mathbf{s}\|_2$ to be small. We can compute the solution to (11) in closed form as $\mathbf{p}^* = \left(\mathbf{Q}^T\mathbf{Q} + \tau\mathbf{A}^H\mathbf{A}\right)^{-1}\mathbf{Q}^T\mathbf{y}$. Then the right hand side of (3) can be obtained as $\mathbf{A}\mathbf{p}^*$, which gives a rough estimate of the source term. Therefore, letting $\mathbf{w}(\mathbf{x}) = \mathbf{A}\mathbf{p}^* \in \mathbb{C}^n$, an initial estimate for the source can be found through thresholding as $\hat{\mathbf{w}}(\mathbf{x}) = |\mathbf{w}(\mathbf{x})|$ if $|\mathbf{w}(\mathbf{x})| > \alpha|\mathbf{w}|_{max}$ and 0 otherwise with $\alpha \in (0,1)$, where $|\cdot|_{max}$ refers to the maximum complex scalar magnitude across all entries of $\mathbf{w}(\mathbf{x})$. We threshold the magnitude of the complex field $\mathbf{w}(\mathbf{x})$ and look at the coordinates $\mathbf{x} \in \mathbb{R}^3$ of the nonzero entries in $\hat{\mathbf{w}}(\mathbf{x})$. A simple clustering algorithm can be applied to these nonzero nodes to determine the possible number of sources and their center locations. Furthermore, since $\mathbf{w}(\mathbf{x})$ is a complex-valued field, it informs not only the initialization of the locations of the sources, but also the relative phase of each source, i.e., the phase of β_i. After performing the clustering to determine possible locations, we take the estimated center coordinate $\mathbf{x}_{0i}$ for source i and calculate the phase of the field $\angle(\mathbf{w}(\mathbf{x}_{0i}))$ at the point $\mathbf{x}_{0i}$ for each source. Source intensities $\beta_i \in \mathbb{C}$ are initialized with magnitude 1 and this corresponding phase.

[1] Forming $\mathbf{A}^{-1}$ would be equivalent to n linear systems solves of size n.

Fig. 1: Experimental setup. Pictured are two speakers (sources), two reflecting walls.

IV. Experimental Results

A. Experiment Setup

Experiments were performed in an anechoic chamber which simulates a free-field environment. Acoustic waves impinging on the wall are absorbed by foam and not reflected back into the chamber. In order to make the domain more interesting, two eight by four foot MDF wood panels were placed in the domain to create acoustic reflecting surfaces. A tool box was also placed within the domain making it a non-convex mesh and introducing more multi path propagation and reflecting surfaces. The setup is displayed in Figure 1.

Time harmonic fields were generated using two Optimus XTS 40 speakers. The speakers were driven with a mixture of pure sine wave tones from a Data Translation DT9857E signal conditioning board. Four half-inch free-field polarized microphones Model 377B02 from PCB electronics were utilized to take the acoustic pressure measurements. Only four microphones were available for the experiment, however localization of multiple sources in complex domains requires more than four measurements of the acoustic field. In order to overcome this equipment limitation, multiple trials were run in which a stand with four microphones placed at different vertical positions was moved to different locations in the domain. For each trial, the speakers received the same driving signal from the signal conditioning board and therefore the recorded signals could be synchronized in time across the different trials making it appear that the microphones across different trials were all recording the same experiment. For each trial, the speakers started emitting while the microphones started recording at time $t = 0$. We allowed the domain to reach steady state and then selected the same two-second time slice of the recording on each microphone. After taking the FFT of the microphone signal, the specific frequency of interest can be extracted from each microphone to create the complex acoustic pressure measurement vector $\mathbf{y}$ used as the input data to the optimization problem (7).

Since the source identification problem is solved using complex pressure measurements in the frequency domain, both the magnitude and the phase of the pressure measurements is important information for solving the problem. Therefore, without time synchronization of the measurements across the different trials, the phase difference that would exist across measurements would affect the obtained solutions. The coordinates of the measurement locations as well as the coordinates of the speakers were measured using 8 OptiTrack localization cameras installed along the top edge of the walls in the anechoic chamber.

B. Source Model

Across all experiments, 400 Hz was utilized as the input frequency for the model (3) and the frequency component to extract from the FFT for the measurement vector $\mathbf{y}$. In general, lower frequencies translate to coarser FE meshes needed to accurately capture the acoustic field, which speeds up computation. The selected frequency translates to a wavelength $\lambda \approx 0.85$ meters, which is large in comparison to the size of the speaker generating the sound. For this reason, the speakers can be treated as monopole radiators that radiate acoustic energy equally in all directions [19]. This uniform directivity was tested and verified in experiment. This motivated the use of a Gaussian-like basis function $g(\mathbf{x};\boldsymbol{\theta}_i)$ in equation (5) to model the sources, given as, $g(\mathbf{x};\boldsymbol{\theta}_i) = \exp\{\lambda_i\|\mathbf{x}-\mathbf{c}_i\|^2\}$, where $\boldsymbol{\theta}_i = [\mathbf{c}_i, \lambda_i]^T$. The parmeter $\mathbf{c}_i \in \mathbb{R}^3$ defines the source location, i.e. where the value of $g(\mathbf{x};\boldsymbol{\theta}_i)$ is maximum, and the parameter $\lambda_i \in \mathbb{R}_{++}$ defines the "spread" of the source, or how fast the intensity decays as you move away from the source's center. Although this source basis function is nonzero over the whole domain Ω, for practical purposes, its value can be considered zero far enough from the center. From a computational perspective, this source model is simple and differentiable with respect to its parameters.

Given this source model, solving the acoustic source identification problem amounts to minimizing (7) with respect to $[\boldsymbol{\theta}_1, \boldsymbol{\beta}_1, \ldots, \boldsymbol{\theta}_k, \boldsymbol{\beta}_k]^T \in \mathbb{R}^{6\times k}$. In order to solve problem (7) numerically, we utilized Matlab's *fmincon* nonlinear constrained optimization package. A trust region algorithm was utilized in which we supplied the gradient and Hessian information. Derivation of the Hessian is omitted for brevity. We placed bound constraints on the location parameters $\mathbf{c}_i \in \Omega$ to reside in the domain as well as bound constraints on the intensities and spread parameters.

C. Multiple-Source Free-Field Results

As a first test of our method, we took measurements without any obstacles in the domain to simulate a free-field environment. We modeled the domain as a 3D rectangular prism with

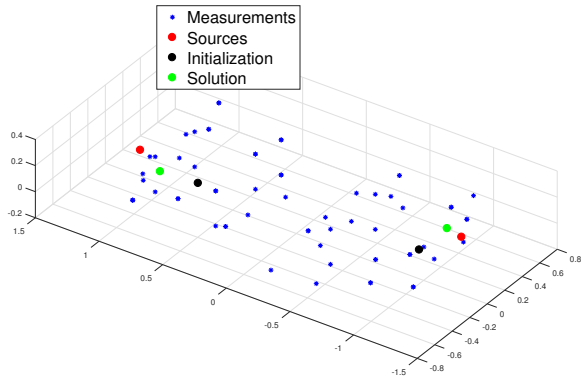

Fig. 2: Free-field domain with two sources using 64 measurements.

# of measurements	64	125	196
source 1 initial error	14.2 %	9.1 %	4.9 %
source 1 final error	6.2 %	3.9 %	2.4 %
source 2 initial error	9.1 %	7.7 %	10.5 %
source 2 final error	3.1 %	2.7 %	1.8 %

TABLE I: Source Localization error vs. number of measurements used for free-field domain.

dimensions $[-0.65, 0.65] \times [-1.65, 1.65] \times [-0.25, 0.25]$ in meters with a mesh with roughly 40,000 nodes. The Sommerfeld radiation condition was enforced on all boundaries. We positioned two speakers at either end of the domain and took measurements of the pressure field in between the speakers. The microphone stands were moved between trials so as to create a uniform collection of measurement points throughout the domain. A total of 196 locations were taken for this experiment. Results for using 64 of the 196 measurements are shown in Figures 2 - 3. The 64 measurements were selected as a uniform grid from the 196 available measurements. Figure 2 shows the localization results for the two sources. Figure 3(a) shows a color map of the magnitude of the complex pressure at the measurement points coming from the experiment and Figure 3(b) shows the magnitude of the field from doing a forward solve of the PDE given the returned source solution from the optimization algorithm. The color maps show good agreement meaning the algorithm is correctly finding sources that match the measured field.

The reduction in localization error for each source is summarized in Table I. This error was calculated by dividing the distance from the true source location for each source by the characteristic size of the domain ℓ, taken to be the distance between opposite corners of the domain. Specifically, the error, err, was calculated as $err = \|\mathbf{c}_i - \mathbf{c}_{true}\|_2/\ell$. The error was calculated for the initial source locations returned from the initialization procedure outlined in Section III-C as well as the error in the returned solution of the optimization problem (7). It can be seen that the algorithm correctly reduces the initial localization error with better reduction when more measurements are used.

The results presented for the two source, free-field case thus far were for an experiment where the two speakers were driven in phase. By switching the positive and negative connections for one of the speakers, the two speakers were driven 180

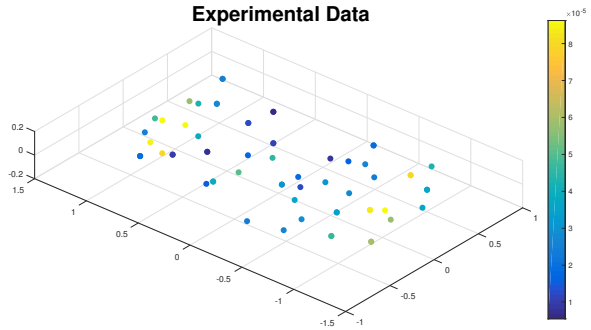

(a)

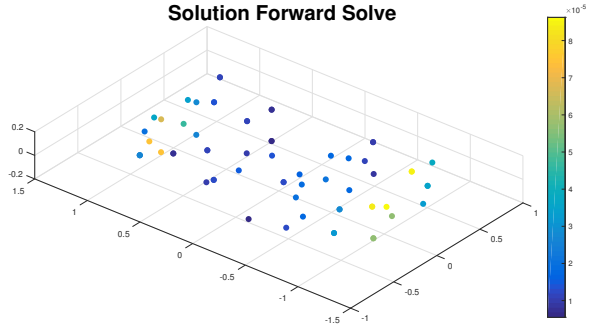

(b)

Fig. 3: Magnitude of complex pressure at 64 measurements locations for free field domain. (a) shows the pressure magnitudes from the experiment. (b) shows the pressure magnitudes at the measurement locations after doing a forward PDE solve given the returned solution. Good agreement can be seen between solution and experimental data.

	In-Phase	180 Degrees Out of Phase
Phase β_1	-83.4	112.5
Phase β_2	-75.0	-122.5
Phase Difference	8.4	235.2

TABLE II: Relative phase difference of free-field experiment with two sources.

degrees out of phase, resulting in a different pressure field. Using the same set of measurement locations, but with the speakers driven out of phase, our algorithm was able to correctly detect this difference and optimize the β_i's accordingly. The results of the relative phase difference between the sources is summarized in Table II.

D. Multiple-Source Non-Free-Field Results

With the experimental setup shown in Figure 1, measurements were taken at 248 locations in the domain. This domain was also modeled as a rectangular prism of dimensions $[0, 2.36] \times [0, 1.14] \times [0, 2.82]$ in meters with a mesh of approximately 20,000 nodes. The sound-hard Neumann boundary condition was applied to the portions of the wall with the MDF wood panels as well as the surface of the tool box. The Sommerfeld radiation condition was applied to all other parts of the boundary, i.e., the boundaries consisting of absorbing foam. As expected in a more complex domain, many measurements of the field are needed to resolve ambiguities in possible source locations. With few number of measurements, higher readings near reflecting boundaries could be interpreted as being close

# of measurements	163	248
source 1 initial error	8.2 %	8.0 %
source 1 final error	6.8%	5.8 %
source 2 initial error	4.3 %	4.5 %
source 2 final error	5.7 %	5.0 %

TABLE III: Source Localization error vs. number of measurements used for non-free-field domain.

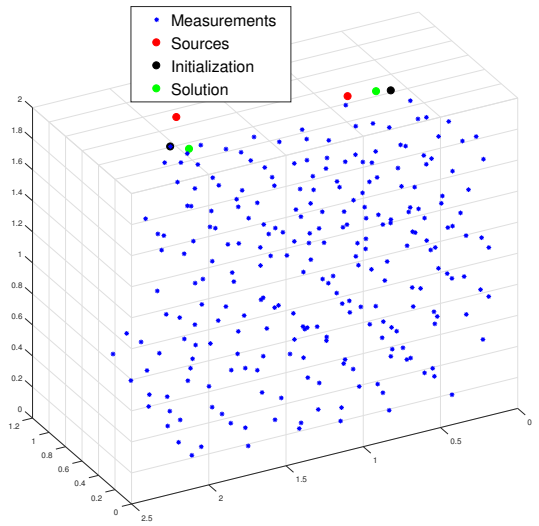

Fig. 4: Non-free-field domain with two sources using 248 measurements.

to the source, and without a good distribution of measurement locations throughout the domain, the optimization algorithm will not be able to properly localize the sources. The use of the PDE resolves these ambiguities but, measurements are still necessary at critical parts of the domain. Results in the localization error are shown in Figure 4 with tabulated errors in Table III. Compared to the free-field case, more measurements were needed in order to obtain a good source estimate. This makes sense given the complex pressure field caused by the reflecting obstacles in the domain. The initialization procedure was observed to be critical for the correct identification of the sources. Even with a good location initialization on the sources, incorrect phase initialization on the intensities β_i could cause the optimization algorithm to drift to undesirable local minima.

V. Conclusion

In this paper we presented a method for solving acoustic source identification problems in the frequency domain given a finite element model of the domain and a set of noisy pressure measurements. We formulated the problem as a least squares optimization problem that minimizes the discrepancy between the observed pressure measurements and those predicted by the governing PDE model. Through real experiments, we were able to show that our method can localize multiple sources in a complex domain with a sufficient number of measurements. Moreover, we can identify more details of the source field, such as relative phase between sources. While simpler methods exist for free-field domains requiring fewer measurements, the approach presented in this paper generalizes to any domain with arbitrary shape and boundary conditions. Furthermore, there is no need to compute response matrices or transfer functions for every potential source location making the approach very versatile.

Acknowledgements

The authors would like to thank Dr. Donald Bliss and Dr. David Raudales for their support and for lending us their lab.

References

[1] R. Khodayi-mehr, W. Aquino, and M. M. Zavlanos, "Nonlinear reduced order source identification," in *American Control Conference (ACC), 2016*, pp. 6302–6307, IEEE, 2016.

[2] R. Khodayi-mehr, W. Aquino, and M. M. Zavlanos, "Model-based active source identification in complex environments," *arXiv preprint arXiv:1706.01603*, 2017.

[3] L. Calkins, R. Khodayi-mehr, W. Aquino, and M. Zavlanos, "Stochastic model-based source identification," in *Decision and Control (CDC), 2017 IEEE 56th Annual Conference on*, pp. 1272–1277, IEEE, 2017.

[4] J. C. Murray, H. Erwin, and S. Wermter, "Robotics sound-source localization and tracking using interaural time difference and cross-correlation," in *AI Workshop on NeuroBotics*, 2004.

[5] J.-M. Valin, F. Michaud, J. Rouat, and D. Létourneau, "Robust sound source localization using a microphone array on a mobile robot," in *Intelligent Robots and Systems, Proceedings. IEEE/RSJ International Conference on*, vol. 2, pp. 1228–1233, IEEE, 2003.

[6] J. Huang, T. Supaongprapa, I. Terakura, F. Wang, N. Ohnishi, and N. Sugie, "A model-based sound localization system and its application to robot navigation," *Robotics and Autonomous Systems*, vol. 27, no. 4, pp. 199–209, 1999.

[7] R. Schmidt, "Multiple emitter location and signal parameter estimation," *IEEE Transactions on Antennas and Propagation*, vol. 34, no. 3, pp. 276–280, 1986.

[8] K. Nakamura, K. Nakadai, and G. Ince, "Real-time super-resolution sound source localization for robots," in *Intelligent Robots and Systems, IEEE/RSJ International Conference on*, pp. 694–699, IEEE, 2012.

[9] S. Argentieri, P. Danès, and P. Souères, "A survey on sound source localization in robotics: From binaural to array processing methods," *Computer Speech & Language*, vol. 34, no. 1, pp. 87–112, 2015.

[10] M. Fink, D. Cassereau, A. Derode, C. Prada, P. Roux, M. Tanter, J.-L. Thomas, and F. Wu, "Time-reversed acoustics," *Reports on Progress in Physics*, vol. 63, no. 12, p. 1933, 2000.

[11] D. G. Albert, L. Liu, and M. L. Moran, "Time reversal processing for source location in an urban environment a," *The Journal of the Acoustical Society of America*, vol. 115, no. 2, pp. 2596–619, 2005.

[12] S. Yon, M. Tanter, and M. Fink, "Sound focusing in rooms: The time-reversal approach," *The Journal of the Acoustical Society of America*, vol. 113, no. 3, pp. 1533–1543, 2003.

[13] S. Kitić, L. Albera, N. Bertin, and R. Gribonval, "Physics-driven inverse problems made tractable with cosparse regularization," *IEEE Transactions on Signal Processing*, vol. 64, no. 2, pp. 335–348, 2016.

[14] S. Nam and R. Gribonval, "Physics-driven structured cosparse modeling for source localization," in *Acoustics, Speech and Signal Processing, IEEE International Conference on*, pp. 5397–5400, IEEE, 2012.

[15] S. Kitic, N. Bertin, and R. Gribonval, "Hearing behind walls: localizing sources in the room next door with cosparsity," in *Acoustics, Speech and Signal Processing, IEEE International Conference on*, pp. 3087–3091, IEEE, 2014.

[16] N. Antonello, T. van Waterschoot, M. Moonen, and P. A. Naylor, "Source localization and signal reconstruction in a reverberant field using the fdtd method," in *Signal Processing Conference, Proceedings of the 22nd European*, pp. 301–305, IEEE, 2014.

[17] I. Dokmanić and M. Vetterli, "Room helps: Acoustic localization with finite elements," in *Acoustics, Speech and Signal Processing, IEEE International Conference on*, pp. 2617–2620, IEEE, 2012.

[18] W. Desmet and D. Vandepitte, "Finite element modeling for acoustics,"

[19] L. E. Kinsler, A. R. Frey, A. B. Coppens, and J. V. Sanders, "Fundamentals of acoustics," *Fundamentals of Acoustics, 4th Edition, by Lawrence E. Kinsler, Austin R. Frey, Alan B. Coppens, James V. Sanders, pp. 560. ISBN 0-471-84789-5. Wiley-VCH, December 1999.*, p. 560, 1999.